Atmos. Chem. Phys. Discuss., https://doi.org/10.5194/acp-2018-1258
Manuscript under review for journal Atmos. Chem. Phys.
Discussion started: 10 December 2018

Atmospheric Chemistry and Physics Discussions

Photooxidants from Brown Carbon and Other Chromophores in Illuminated Particle Extracts

Richie Kaur[1], Jacqueline R. Labins[1], Scarlett S. Helbock[1], Wenqing Jiang[2], Keith J. Bein[3], Qi Zhang[2], Cort Anastasio[1,*]

[1]Department of Land, Air and Water Resources, University of California-Davis, One Shields Avenue, Davis, CA 95616-8627, USA

[2]Department of Environmental Toxicology, University of California-Davis, One Shields Avenue, Davis, CA 95616-8627, USA

[3]Center for Health and the Environment, University of California-Davis, One Shields Avenue, Davis, CA 95616-8627, USA

Correspondence to: C. Anastasio (canastasio@ucdavis.edu)

Abstract

While photooxidants are important in atmospheric condensed phases, there are very few measurements in particulate matter (PM). Here we measure light absorption and the concentrations of three photooxidants – hydroxyl radical ($^{\bullet}$OH), singlet molecular oxygen ($^1O_2$*) and oxidizing triplet excited states of organic matter (^{3}C*) – in illuminated aqueous extracts of wintertime particles from Davis, California. $^1O_2$* and $^3C^*$, which are formed from photoexcitation of brown carbon (BrC), have not been previously measured in PM. In the extracts, mass absorption coefficients for dissolved organic compounds (MAC_{DOC}) at 300 nm range between 13,000–30,000 cm^2 $g\text{–}C^{-1}$ and are approximately twice as high as previous values in Davis fogs. The average (± 1σ) $^{\bullet}$OH steady-state concentration in particle extracts is 4.7 (± 1.9) × 10^{-16} M, which is very similar to previous values in fog, cloud and rain: although our particle extracts are more concentrated, the resulting enhancement in the rate of $^{\bullet}$OH photoproduction is essentially cancelled out by a corresponding enhancement in concentrations of natural sinks for $^{\bullet}$OH. In contrast, concentrations of the two oxidants formed primarily from brown carbon (i.e., $^1O_2$* and ^{3}C*) are both enhanced in the particle extracts compared to Davis fogs, a result of higher concentrations of dissolved organic carbon and faster rates of light absorption in the extracts. The average $^1O_2$* concentration in the PM extracts is 1.6 (± 0.5) × 10^{-12} M , seven times higher than past fog measurements, while the average concentration of oxidizing triplets is 1.0 (± 0.4) × 10^{-13} M, nearly double the average Davis fog value.

Atmos. Chem. Phys. Discuss., https://doi.org/10.5194/acp-2018-1258
Manuscript under review for journal Atmos. Chem. Phys.
Discussion started: 10 December 2018

Atmospheric Chemistry and Physics Discussions

Additionally, the rates of $^1O_2$* and ^{3}C* photoproduction are both well correlated with the rate of sunlight absorption.

While concentrations of $^1O_2$* and $^3C^*$ are higher in our PM extracts compared to fog, the extracts are approximately 1000 times more dilute than water-containing ambient PM. Since we cannot experimentally measure photooxidants under these ambient conditions, we measured the effect of PM dilution on oxidant concentrations and then extrapolated to ambient particle conditions. As the particle mass concentration in the extracts increases, measured concentrations of $^{\bullet}$OH remain relatively unchanged, $^1O_2$* increases linearly, and ^{3}C* concentrations increase less than linearly, likely due to quenching by dissolved organics. Based on our measurements, and accounting for additional sources and sinks that should be important under PM conditions, we estimate that [$^{\bullet}$OH] in particles is essentially the same as in fog waters, [^{3}C*] is higher in PM by nearly a factor of 3, and [$^1O_2$*] is enhanced by a factor of roughly 600. Because of these enhancements in $^1O_2$* and $^3C^*$ concentrations, the lifetimes of some highly soluble organics appear to be much shorter in particle liquid water than under foggy/cloudy conditions. Based on our extrapolated rates of formation, BrC-derived singlet molecular oxygen and triplet excited states are the dominant sinks for organic compounds in particle liquid water, with an aggregate rate of reaction for each oxidant that is approximately 200 – 300 times higher than the aggregate rate of reactions for organics with $^{\bullet}$OH. For individual, highly soluble reactive organic compounds it appears that $^1O_2$* is the major sink in particle water. Triplet excited states are likely also important in the fate of individual particulate organics, but assessing this requires additional measurements of triplet interactions with dissolved organic carbon in natural samples.

1 Introduction

Photochemically generated oxidants largely drive atmospheric chemistry, both in the gas phase (Thompson, 1992; Finlayson-Pitts and Pitts Jr, 1999; Seinfeld and Pandis, 2012) and in aqueous drops, where they largely govern the reactions and lifetimes of organic compounds (Lim et al., 2005; Lim et al., 2010; Ervens et al., 2011; He et al., 2013; Herrmann et al., 2015; Blando and Turpin, 2000). Similarly, photooxidants can be important for transformations in water-containing particulate matter (PM): they make new PM mass by functionalizing gaseous volatile organics to oxygenated lower-volatility products, and decrease PM mass by fragmenting large organics into smaller, more volatile species (Jimenez et al., 2009). Oxidants in condensed phases can come from the gas phase (e.g., the mass transport of hydroxyl radical, $^{\bullet}$OH) or can be formed

photochemically within the particle or drop (Herrmann et al., 2010). Our focus in this paper is on the latter pathway.

Of the photooxidants formed in airborne particles, hydroxyl radical ($^{\bullet}$OH) is the most widely studied. While its concentrations have been measured in cloud/fog drops, rain and dew (Arakaki and Faust, 1998; Arakaki et al., 1999; Anastasio and McGregor, 2001; Kaur and Anastasio, 2017), there are only four known measurements of $^{\bullet}$OH photoproduction rates, lifetimes, and steady-state concentrations in ambient particles, all from coastal or marine locations (Anastasio and Jordan, 2004; Arakaki et al., 2006; Anastasio and Newberg, 2007; Arakaki et al., 2013). Based on these and other measurements (e.g., Tong et al. (2017)) and complementary modeling work (Herrmann et al., 2010; Herrmann et al., 2015), the major sources of $^{\bullet}$OH include photolysis of nitrate, nitrite, and hydrogen peroxide (HOOH) as well as reactions of Fe(II) with HOOH or organic peroxides.

Photoexcitation of organic chromophores, i.e., light-absorbing brown carbon (BrC), can also form oxidants in particles and drops. For example, sunlight absorption by organic chromophores can promote the molecules from their ground states to reactive triplet excited states (McNeill and Canonica, 2016; Kaur and Anastasio, 2018b). Triplets can both directly oxidize organics via electron transfer reactions and form other photooxidants, including singlet molecular oxygen ($^1O_2$*) (Zepp et al., 1985) and hydrogen peroxide (Anastasio et al., 1997). In this work we examine oxidizing triplets, which we refer to as $^3C^*$ or simply "triplets" for simplicity. Such species are important in surface waters, where they rapidly oxidize several classes of compounds including phenols, anilines, phenylurea herbicides, and sulfonamide antibiotics (Canonica et al., 1995; Canonica and Hoigné, 1995; Boreen et al., 2005; Canonica et al., 2006; Bahnmüller et al., 2014).

There has been growing interest in the role and reactivity of triplets formed from particulate brown carbon, especially their role in forming aqueous secondary organic aerosol (SOA(aq))(Smith et al., 2014; 2015; Yu et al., 2014; Yu et al., 2016; Laskin et al., 2015). There is evidence that triplet-forming, light-absorbing species, e.g., imidazoles and pyrazines, are formed in drops and particles (De Haan et al., 2009; 2010; Hawkins et al., 2018) and a few laboratory studies have examined how illuminated imidazole particles can oxidize isoprene or other alkenes to increase PM mass (Aregahegn et al., 2013; Rossignol et al., 2014). But the formation of SOA(aq) from such reactions appears not to be significant under environmentally relevant conditions where concentrations of triplet precursors are much lower (Tsui et al., 2017). While we recently made the first measurements of triplet concentrations in fog waters (Kaur and

Anastasio, 2018b), there are no measurements of $^3C^*$ in particles, making it difficult to assess their significance. This is doubly difficult because triplets are not a single oxidant, but rather a suite of species with a wide range of reactivities (McNeill and Canonica, 2016).

Another important photooxidant in atmospheric and surface waters is singlet molecular oxygen ($^1O_2^*$), which is formed by energy transfer from a triplet excited state to dissolved oxygen, and lost via deactivation by water (Zepp et al., 1977; Haag and Hoigné, 1986; Haag and Gassman, 1984; Faust and Allen, 1992). Similar to triplets, singlet oxygen has been studied widely in surface waters (Zepp et al., 1977; Haag and Gassman, 1984; Haag and Hoigné, 1986; Tratnyek and Hoigné, 1994) and reacts rapidly with electron-rich organics such as phenols, polycyclic aromatic hydrocarbons, amino acids, and reduced sulfur species (Wilkinson et al., 1995). However, there are only four measurements of $^1O_2^*$ concentrations in atmospheric waters (Anastasio and McGregor, 2001; Kaur and Anastasio, 2017; Albinet et al., 2010; Faust and Allen, 1992) and none in aqueous particles.

To address this gap, we measured $^{\bullet}OH$, $^1O_2^*$, and $^3C^*$ in illuminated aqueous extracts of fine particles collected from the Central Valley of California during winter, a period of heavy residential wood burning. The goals of this study are to: 1) quantify $^{\bullet}OH$, $^1O_2^*$, and $^3C^*$ kinetics and concentrations in particle extracts, 2) compare light absorption and photooxidant kinetics with previous measurements made in fog, 3) measure the dependence of oxidant concentrations on particle dilution to predict photooxidant concentrations in ambient particle liquid water, and 4) assess the importance of particle photooxidants in processing organic compounds in the atmosphere.

2 Experimental

2.1 Chemicals

All chemicals were used as received. Furfuryl alcohol (98%), syringol (99%), methyl jasmonate (95%), benzene (≥ 99.9%), 2-methyl-3-buten-2-ol (98%), deuterium oxide (99.9% atom D), and 2-nitrobenzaldehyde (98%) were from Sigma-Aldrich and sulfuric acid (trace metal grade) was from Fisher. All chemical solutions and particulate matter extracts were prepared using purified water (Milli-Q water) from a Milli-Q Advantage A10 system (Millipore; ≥ 18.2 MΩ cm) with an upstream Barnstead activated carbon cartridge; total organic carbon concentrations were below 10 ppb C.

2.2 Particle collection and extraction

Wintertime particles were collected in a residential neighborhood in Davis, California, (38.5539° N, 121.7381° W, 16 m above sea level) during December 2015 and January 2016, a period with significant wood burning. $PM_{2.5}$ was collected on 8 × 10 inch Teflon-coated quartz filters (Pall Corporation, EmFab™ filters, type TX40HI20-WW) using a high-volume sampler with a PM_{10} inlet (Graseby Anderson) followed by two offset, slotted impactor plates (Tisch Environmental, Inc., 230 series) to remove particles greater than 2.5 μm. Due to technical difficulties, the air flow rate was variable and typically ranged between 1130 and 1560 L min^{-1}, corresponding to particle cut points of 2.5 to 1.6 μm. Particles were generally collected over two to three consecutive nights between 5:30 pm and 7:30 am, but one sample (#3) was collected continuously (day and night) for 72 hours (Table S1).

Immediately upon collection, samples were wrapped in aluminum foil (previously baked at 500 °C for 8 h), sealed in Ziplock™ bags and stored at –20 °C. On the day of extraction, several 2 cm × 2 cm pieces were cut (using stainless-steel tools) from the same filter, each was put into a separate pre-cleaned 10 mL amber glass vial, Milli-Q water was added (see below), and the vial was sealed and shaken for 3 hours in the dark. The extracts were filtered (0.22 μm PTFE ; Pall), combined, and labeled as Particulate Matter Extract (PME). The standard condition was to use 1.0 mL of Milli-Q to extract each filter square, but in our initial work we used 2.5 mL of Milli-Q per filter square; these latter "dilute extracts" are indicated by an asterisk and footnotes in the figures and tables. To study the effect of PM mass concentration, separate portions of filter #3 were extracted using five different extraction volumes between 0.5 and 10 mL (discussed later). Those extracts are labeled as PME3Dx, where "x" is the extraction volume (e.g., PME3D1.3 for filter squares extracted in 1.3 mL of Milli-Q). Upon extraction, each PME was stored in the refrigerator (5 °C) until the day of the illumination experiments. All illumination experiments and analyses on a PME sample were completed within a week of its extraction.

2.3 Sample illumination and chemical analysis

For all illumination experiments except P_{OH} measurements (discussed below), on the day of the experiment a 1.0 mL aliquot of an air-saturated particle extract was first acidified to pH 4.2 ± 0.2 using 10 mM sulfuric acid to mimic the particle water acidity in wintertime PM in California's Central Valley (Parworth et al., 2017). The acidified extract was then spiked with a single photooxidant probe and put into a silicone-plugged, fully-filled GE021 quartz tube (4 mm inner diameter, 6 cm length, 1.0 mL volume) and illuminated with a 1000 W xenon arc lamp

filtered with a water filter (to reduce sample heating), an AM 1.0 air mass filter (AM1D-3L, Sciencetech) and 295 nm long-pass filter (20CGA-295, Thorlabs) to mimic tropospheric solar light (Kaur and Anastasio, 2017). Because of the small tube size, samples were not stirred, but the entire sample was illuminated in a chamber held at 20 °C. 100 µL aliquots of illuminated (and parallel dark) samples were periodically removed and analyzed for the concentration of photooxidant probe (see below) using HPLC (Shimadzu LC-10AT pump, ThermoScientific BetaBasic-18 C_{18} column (250 × 33 mm, 5 µM bead), and Shimadzu-10AT UV-Vis detector). The photon flux in the sample was measured on each experiment day using a 10 µM solution of 2-nitrobenzaldehyde (2NB) in the same type of quartz tube as the sample (Galbavy et al., 2010).

Major anions and cations in the extracts (Table S2) were quantified using two Metrohm ion chromatographs (881 Compact IC Pro) equipped with conductivity detectors (Ge et al., 2014; Kaur and Anastasio, 2017). Dissolved organic carbon (DOC) in the filtered extracts was measured using a Shimadzu TOC-VCPH analyzer (Yu et al., 2014).

2.4 Light Absorbance

Light absorbance was measured immediately after extraction using a Shimadzu UV-2501PC spectrophotometer with 1-cm quartz cuvettes and a baseline of Milli-Q water. Absorbance (A_λ) was converted to light absorption coefficients using

$$\alpha_\lambda = \frac{A_\lambda}{l} \quad (1)$$

where l is the pathlength. The rate of sunlight absorption (R_{abs}, mol-photons L^{-1} s^{-1}) in each extract was calculated as:

$$R_{abs} = 2.303 \times \frac{10^3}{N_A} \times \sum_{300nm}^{450nm} (\alpha_\lambda \times I_\lambda \times \Delta\lambda) \quad (2)$$

where 2.303 is for base conversion, 10^3 is for units conversion (cm^3 L^{-1}), N_A is Avogadro's number, I_λ is the Davis winter-solstice actinic flux (photons cm^{-2} s^{-1} nm^{-1}) from the Tropospheric Ultraviolet and Visible (TUV) Radiation Model version 4.1 (Madronich et al., 2002), and $\Delta\lambda$ is the interval between adjacent wavelengths in the TUV output (nm).

Wavelength-dependent mass absorption coefficients for DOC (MAC_{DOC}; cm^2 g–C^{-1}) were estimated by subtracting the contributions of nitrite and nitrate from the measured absorbance at each wavelength and then dividing the remainder by the DOC concentration:

Atmos. Chem. Phys. Discuss., https://doi.org/10.5194/acp-2018-1258
Manuscript under review for journal Atmos. Chem. Phys.
Discussion started: 10 December 2018

Atmospheric Chemistry and Physics Discussions

$$MAC_{DOC,\lambda} = \frac{\alpha_{DOC,\lambda} \times ln(10) \times 10^3 \times 10^3}{[DOC]} \quad (3)$$

where $\alpha_{DOC,\lambda}$ (cm^{-1}) is the sample absorbance coefficient at wavelength λ due to DOC (Kaur and Anastasio (2017)); ln(10) is a base conversion factor; the two 10^3 factors are for unit conversion (cm^3 L^{-1} and mg g^{-1}), and the DOC concentration is in mg-C L^{-1}. Since the average OM/OC ratio in California Central Valley particles is approximately 1.7 (Young et al., 2016), the absorption coefficients normalized by OM mass will be approximately 60% of the MAC_{DOC} values.

2.5 Measurement of photooxidants

2.5.1 Hydroxyl radical (•OH)

We quantified •OH kinetics using a benzene probe (Zhou and Mopper, 1990; Anastasio and McGregor, 2001; Kaur and Anastasio, 2017). Briefly, four aliquots of each extract were spiked with varying concentrations of benzene to trap •OH and form phenol, which is quantified (Fig. S1). Each benzene stock was made a day before the illumination experiment. Similar to the other photooxidant experiments, all aliquots were air-saturated, acidified to an initial pH of 4.2 (± 0.2), capped, and then constantly stirred during illuminated in airtight 5.0 mL, 1-cm pathlength, rectangular quartz cuvettes with no initial headspace. Throughout the illumination period, 100 µL aliquots were collected through the cap septum and analyzed for phenol using HPLC-UV (eluent of 30% acetonitrile: 70% Milli-Q, flow rate of 0.6 mL/min, detection wavelength of 210 nm and column temperature of 35°C). As described in Kaur and Anastasio (2017), we use these results to determine three experimental quantities for •OH: the rate of photoproduction ($P_{OH,EXP}$), the rate constant for •OH loss due to natural sinks (k'_{OH}), and the steady-state concentration ($[•OH]_{EXP}$). Measured rates of •OH formation and steady-state concentrations were normalized to values expected under midday, Davis winter-solstice sunlight and were corrected for the small amount of internal light screening due to light absorption by DOM:

$$[•OH] = \left(\frac{[•OH]_{EXP}}{S_\lambda \times j_{2NB,EXP}}\right) \times j_{2NB,WIN} \quad (4)$$

In this equation, S_λ is the internal light screening factor (Table S1), $j_{2NB,WIN}$ is the rate constant for loss of 2-nitrobenzaldehyde at midday near the winter solstice in Davis (solar zenith angle =

214 62°, $j_{2NB,WIN}$ = 0.0070 s^{-1}; Anastasio and McGregor, (2001)), and $j_{2NB,EXP}$ is the measured rate
215 constant for loss of 2NB on the day of the experiment.

216 We also measured •OH steady-state concentrations in squares of particle filter #3 using
217 five different dilutions with water (discussed later). Because these sample volumes were too
218 small to use the benzene technique, we measured the steady-state concentration of •OH using 2-
219 methyl-3-buten-2-ol (MBO) (Sect. S1). We then measured P_{OH} in a cuvette using a high benzene
220 concentration (1.5 mM) and determined the rate constant for •OH loss due to natural sinks by
221 dividing the rate of photoproduction by the steady-state concentration, $k'_{OH} = P_{OH} / [^{\bullet}OH]$ (Sect.
222 S1.3). •OH results are in Tables S3–S6.

223 **2.5.2 Singlet molecular oxygen ($^1O_2$*)**

224 Singlet oxygen was quantified by measuring the loss of a furfuryl alcohol (FFA) probe
225 and using heavy water (D_2O) as a diagnostic tool (Kaur and Anastasio, 2017; Anastasio and
226 McGregor, 2001). Briefly, each extract was divided into two aliquots, acidified to pH 4.2 (± 0.2),
227 and diluted 50:50 using H_2O or D_2O. Both aliquots were spiked to 10 μM FFA and illuminated
228 in 1 mL quartz tubes. FFA loss was detected using HPLC-UV (eluent of 10% acetonitrile: 90%
229 Milli-Q water, flow rate of 0.6 mL/min, detection wavelength of 210 nm and column
230 temperature of 35°C). The loss of FFA followed pseudo-first-order kinetics and the slope of the
231 plot of $\ln([FFA]_t / [FFA]_0)$ versus time is the negative of the pseudo-first-order rate constant for
232 loss of FFA (illustrated in Fig. S2). Loss of FFA in the D_2O-diluted aliquot is faster than in H_2O
233 because H_2O is the dominant sink for $^1O_2$*, which reacts less quickly with D_2O (Bilski et al.,
234 1997). The differences in the pseudo-first-order rate constants for loss of FFA between the two
235 aliquots of sample were used to calculate the steady-state concentration of $^1O_2$* and the rate of
236 singlet oxygen photoproduction (Anastasio and McGregor, 2001). These were normalized to
237 values expected in Davis winter-solstice sunlight (i.e., $[^1O_2^*]$ and P_{1O2*}) and corrected for
238 internal light screening using an equation analogous to Eq. (4). $^1O_2$* measurements are in Table
239 S7.
240

241 **2.5.3 Oxidizing triplet excited states of organic matter (^{3}C*)**

242 Triplets were measured using the dual-probe technique we developed recently for fog
243 waters (Kaur and Anastasio, 2018b): two 1.0 mL, pH 4.2 aliquots of each extract were spiked to
244 10 μM of either syringol (SYR) or methyl jasmonate (MeJA) and the loss of each probe was
245 measured during illumination in plugged quartz tubes (Sect. 2.3). The measured pseudo-first-

Atmos. Chem. Phys. Discuss., https://doi.org/10.5194/acp-2018-1258
Manuscript under review for journal Atmos. Chem. Phys.
Discussion started: 10 December 2018

Atmospheric Chemistry and Physics Discussions

order rate constant for probe loss ($k'_{Probe,EXP}$) was determined as the negative of the slope of the plot of ln([Probe]/[Probe]$_0$) versus illumination time. Values of $k'_{Probe,EXP}$ were normalized to Davis winter-solstice sunlight and corrected for internal light screening using an analog of Eq. (4); the resulting rate constants are termed k'_{Probe} (s^{-1}) (Tables S8, S9 of the SI). This pseudo-first-order rate constant for loss of probe represents the sum of all loss pathways:

$$k'_{Probe} = k_{Probe+OH}[^{\bullet}OH] + k_{Probe+1O2*}[^1O_2*] + \Sigma(k_{Probe+3C_i*}[^3C_i*]) + j_{Probe} + \Sigma(k_{Probe+Other}[Other]) \quad (5)$$

where the first two terms are the contributions of $^{\bullet}OH$ and $^1O_2*$ to probe loss; $\Sigma(k_{Probe+3C*}[^3C*])$ represents the sum of all triplet contributions to probe loss; j_{Probe} is the first-order rate constant for direct photodegradation of the probe, which is negligible for our illumination times (< 4.3 × 10^{-6} s^{-1} and 4.8 × 10^{-7} s^{-1} for SYR and MeJA, respectively, under Davis winter conditions); and $\Sigma(k_{Probe+Other}[Other])$ is the sum of contributions from all other oxidants. As described in Sect. S3, we estimate that these other oxidants (hydroperoxyl radical / superoxide radical anion, ozone, carbonate radical, hydrogen ion / aquated electron) contribute 12 % or less of the average measured syringol loss (Sect. S3) and so are ignored. We can then simplify and rearrange Eq. (5) to determine the triplet contribution to probe loss:

$$k'_{Probe,3C*} = \Sigma(k_{Probe+3Ci*}[^3C_i*]) = k'_{Probe} - (k_{Probe+OH}[^{\bullet}OH] + k_{Probe+1O2*}[^1O_2*]) \quad (6)$$

As a proxy for the complex, unidentified mixture of natural triplets, we use four model triplets – 2-acetonaphthone (^{3}2AN*), 3'-methoxyacetophenone (^{3}3MAP*), 3,4-dimethoxybenzaldehdye (^{3}DMB*), and benzophenone (^{3}BP*) – that roughly span the range of triplet reactivities in natural samples. With our method, we first identify the "best match triplets", i.e., the one or two model triplets that bracket the average oxidizing triplet reactivity in a given extract. To do this, we determine the model triplets where the ratio of measured probe loss rate constants due to triplets ($k'_{SYR,3C*}$ / $k'_{MeJA,3C*}$) in each extract matches the mole-fraction-weighted ratio of the second-order rate constants (i.e., $k_{SYR+3C*}$ / $k_{MeJA+3C*}$) of the best match triplets (Kaur and Anastasio, 2018b). Second-order rate constant ratios of the model triplets range from 1.7 for the most reactive species (^{3}BP*) to 100 for the least reactive, ^{3}2AN* (Table S10). For each extract, we calculated two mole-fraction-weighted second-order rate constants for triplets, one for each probe, and used them to estimate the triplet steady-state concentration:

$$\Sigma[^3C_i*]_{Probe} = \frac{k'_{Probe,3C*}}{\chi_{3C1*} \times k_{Probe+3C1*} + \chi_{3C2*} \times k_{Probe+3C2*}} \quad (7)$$

where χ_{3C1*} and χ_{3C2*} are the mole fractions of the two best match triplets ($^3C_1$* and $^3C_2$*), and $k_{Probe+3C1*}$ and $k_{Probe+3C2*}$ are the second-order reaction rate constants of the best model triplet matches. Eq. (7) gives us two estimates of the triplet steady-state concentration, one from each probe, i.e., $\sum[^3C_i*]_{SYR}$ and $\sum[^3C_i*]_{MeJA}$. We averaged the two to obtain the best value for the triplet steady-state concentration in each extract, $\sum[^3C_i*]$.

We next estimated the rate of triplet photoformation (P_{3C*}):

$$P_{3C*} = \Sigma[^3C_i*] \times (k_{3C*+O2}[O_2] + (k_{rxn} + k_Q)[DOC]) \quad (8)$$

where k_{3C*+O2} is the average bimolecular rate constant for quenching of the model triplets by O_2 (= 2.8×10^9 $M^{-1}s^{-1}$: Table S11 and Canonica et al. (2000)), $[O_2]$ is the dissolved oxygen concentration of 284 μM at 20 °C (USGS, 2018), $k_{rxn} + k_Q$ is the overall reaction and quenching rate constant for triplets by DOC (3.4×10^8 L mol-C^{-1} s^{-1}; see below) and [DOC] values are in Table S2. Measurements for triplets are in Tables S12 and S13.

For all three photooxidants, the quantum yield of formation was calculated as

$$\Phi_{Ox} = \frac{P_{Ox}}{R_{abs}} \quad (9)$$

where P_{OX} is the Davis winter-solstice-normalized rate of oxidant photoproduction and R_{abs} is the rate of sunlight absorption by the extract.

2.5.4 PM mass concentration factor (CF)

Due to the volume required for our probe techniques, we extract particles into Milli-Q water, resulting in extracts that are approximately 1000 times more dilute than ambient particles. To examine the impact of dilution on photooxidant concentrations, we extracted sample #3 in five different volumes of Milli-Q water (0.5 to 10 mL) and measured $^{\bullet}OH$, $^1O_2$* and ^3C* steady-state concentrations in the five extracts. We define the PM mass concentration factor (CF) as the ratio of (PM mass) / (water mass) in a given extract relative to the most concentrated extract that we can make:

$$CF = \frac{V_{MIN}}{V_{EXT}+V_P} \quad (10)$$

where V_{MIN} is the minimum experimentally feasible volume of Milli-Q needed for extraction of one filter square (0.5 mL), V_{EXT} is the volume of Milli-Q used to extract a given filter square (0.5 to 10 mL), and V_P is the volume of probe stock solution added (typically 20 µL). Values of CF for the PME3D extracts ranged from 0.05 (least concentrated) to 0.96 (most concentrated) and are listed in Table S14.

2.5.5 Uncertainties

In figures, error bars represent ± 1 standard error (SE) calculated by propagating the uncertainties in each term used to calculate the plotted value.

3 Results and discussion

3.1 General extract characteristics

Similar to Davis fogs collected in 1997-98 (Anastasio and McGregor, 2001) and 2011 (Kaur and Anastasio, 2017), the most abundant ions in the particle extracts are ammonium (NH_4^+, 280–2600 µM) and nitrate (NO_3^-, 380–3300 µM) (Table S2). This is expected since ammonium nitrate is the most significant inorganic component of wintertime particles in the Central Valley (Herner et al., 2006; Heald et al., 2012; Young et al., 2016). The average values of NO_3^- and NH_4^+ are not statistically different ($p > 0.5$) between the current particle extracts (PME) and previous fogs, although the ranges are much wider in the particle extracts (Table S2). Similar to nitrate, nitrite is another important source of hydroxyl radical in the aqueous phase (Anastasio and McGregor, 2001), with an average concentration of 6.9 (± 2.9) µM in the particle extracts, again statistically similar to the 2011 fog average. On the other hand, the average concentration of potassium – commonly used as a tracer for biomass-burning (Silva et al., 1999; Parworth et al., 2017) – is nearly 40 times higher in the particles than in the 2011 Davis fog samples ($p = 0.019$), suggesting PME enrichment by residential wintertime wood-burning. This is reflected in the dilute PM extracts as well: even though most characteristics in the dilute extracts are similar to fog, the average K^+ (38 ± 7 µM) in the dilute PMEs is 10 times higher than the fog value. Dissolved organic carbon (DOC) in the standard extracts (mean: 3400 (± 760) µM-C) is, on average, three times higher than both the dilute extracts and fog.

We employed two field blanks in this study, one each for dilute and standard extraction conditions. Ions and DOC in both field blanks are lower than 10% of the corresponding PME sample averages, with a few exceptions (Table S2).

Atmos. Chem. Phys. Discuss., https://doi.org/10.5194/acp-2018-1258
Manuscript under review for journal Atmos. Chem. Phys.
Discussion started: 10 December 2018

Atmospheric Chemistry and Physics Discussions

3.2 Light absorption in particle extracts

As shown in Fig. 1a and Table S1, the pathlength-normalized absorbance (α, cm^{-1}) declines exponentially with wavelength, with values at 300 nm (α_{300}) between 0.27 and 0.58 cm^{-1} for the standard extracts PME3–6. The average α_{300} value is nearly five times higher in standard extracts than values in Davis fog samples (Table S1, Fig. S3, data available in Kaur and Anastasio (2018a)), while the "dilute extracts" (PME1*, PME2*, and PME3D2.5*) have absorbances very similar to fog samples. Absorption Angstrom Exponents for all PM extracts range between 6.2 and 7.9 (Table S1), similar to those reported previously for water soluble particulate BrC from biomass burning (Hecobian et al., 2010; Kirchstetter and Thatcher, 2012). For both the fog and PM extracts the calculated rate of sunlight absorption between 300 and 450 nm (R_{abs}) is well-correlated with dissolved organic carbon (DOC) (R^2 = 0.70; Fig. S4), suggesting that BrC is mainly responsible for light absorption. The R_{abs} values for the standard extracts are high, with an average value of 9.1 (± 4.1) × 10^{-6} mol-photons L^{-1} s^{-1}, five times higher than the dilute extracts and past Davis fogs (Table S1). Similar to fog (Kaur and Anastasio, 2018b), the average rate of sunlight absorbance in the standard particle extracts is 17 times higher than the total formation rates of the three photooxidants (discussed later), indicating that most of the (photo) energy absorbed is either dissipated via non-reactive pathways or leads to formation of other products.

We next calculated mass absorption coefficients for the organics (MAC_{DOC}) by subtracting the absorbance contributions by nitrite and nitrate from α and dividing by the DOC concentration (Eq. (3)). Across both standard and dilute extracts, the average (± σ) MAC_{DOC} value at 300 nm is 2.2 (± 0.7) × 10^4 cm^2 g–C^{-1}, 1.7 times higher than the fog sample average (Figs. 1b and S3; data available at Kaur and Anastasio (2018a)). Both α and MAC_{DOC} in the PME are generally higher than in fog, especially at shorter sunlight wavelengths (Fig. S5). Since MAC_{DOC} accounts for dilution (Eq. (3)), the higher values in PM extracts indicates that water-soluble organics in particles are either more strongly light-absorbing (on a per-carbon basis), and/or less diluted with non-absorbing DOC, compared to those in fog. Our PME mass-absorption coefficients at 300 nm are very similar to values reported for the humic–like fraction of biomass-burning aerosols in the Amazon basin (Hoffer et al., 2006) and for the water-soluble organic fractions of rural aerosols (Varga et al., 2001; Sun et al., 2007) .

Compared to the samples, light absorption in the field blanks is negligible, representing 0.7% and 3% of the average α_{300} in the standard and dilute extracts, respectively (Table S1).

Atmos. Chem. Phys. Discuss., https://doi.org/10.5194/acp-2018-1258
Manuscript under review for journal Atmos. Chem. Phys.
Discussion started: 10 December 2018

3.3 Hydroxyl radical

The average Davis winter-solstice-normalized rate of •OH photoproduction (P_{OH}) in the standard extracts is 1.2 (± 0.5) × 10^{-9} M s^{-1} (i.e., 4.2 ± 1.7 μM h^{-1}), 3.3 times faster than the average of previous Davis fogs (Table S3). In Davis fog, the main sources of •OH were nitrite and nitrate photolysis, accounting for 70 – 90 % of measured P_{OH} (Anastasio and McGregor, 2001; Kaur and Anastasio, 2017). However, in the standard PM extracts, nitrite and nitrate together account for an average of only (34 ± 14) % of P_{OH} (Table S4), while other, unidentified species account for the remaining (66 ± 14) %. While NO_2^- and NO_3^- concentrations in PME and fog are similar, measured •OH photoproduction rates are much higher in the particle extracts. The additional sources of •OH likely include photo-Fenton processes (Arakaki and Faust, 1998) and organic peroxides (Tong et al., 2016; Tong et al., 2017; Lim and Turpin, 2015), although there is only a modest correlation between DOC and P_{OH} due to unidentified sources (Fig. S6).

While organic compounds are potentially important sources of •OH in the particle extracts, they are almost certainly the main •OH sink, as found previously for atmospheric and surface waters (Brezonik and Fulkerson-Brekken, 1998; Dong et al., 2010; Arakaki et al., 2013). The average (± 1σ) rate constant for •OH destruction, k'_{OH}, in the standard extracts is 2.6 (± 1.0) × 10^6 s^{-1}, three times higher than in dilute extracts and fog (Table S3); DOC concentrations in the standard PM extracts are similarly enhanced (Table S2). Based on our calculations, inorganic species together account for no more than 10 % of k'_{OH} in the PM extracts (Tables S5, S6). The rate constant for •OH destruction due to organics, i.e., $k'_{OH,org}$, obtained by subtracting contributions of the inorganic sinks from k'_{OH}, is well correlated with DOC concentrations (R^2 = 0.76) (Fig. S6). Arakaki et al. (2013) showed that the ratio $k'_{OH,org}$ / [DOC] is relatively constant in atmospheric waters, with an average (± 1 σ) value of 3.8 (± 1.9) × 10^8 L (mol–C)$^{-1}$ s^{-1}. Our average (± 1σ) measured ratio in all particle extracts is twice as high, 7.6 (± 2.7) × 10^8 L (mol–C)$^{-1}$ s^{-1}, but not statistically different (Table S3).

Davis winter-solstice-normalized •OH steady-state concentrations in all extracts are in the range of (1.7–6.4) × 10^{-16} M, with an average (± 1σ) value of 4.7 (± 1.9) × 10^{-16} M in the standard extracts (Fig. 2a, Table S3). While both the •OH photoproduction rate and rate constant for •OH loss are approximately three times higher in the standard PM extracts compared to the dilute extracts and fog, the two enhancements cancel out to give •OH steady-state concentrations that are similar across all three sample types. This relative consistency of •OH concentrations has been reported for a wide variety of atmospheric waters (Arakaki et al., 2013); our average concentration is similar to most of these past results (Fig. S7). As we discuss in Sect. 3.6,

transport of •OH from the gas-phase is also an important source to particles, increasing the aqueous •OH concentration by approximately 30%.

We also calculated the quantum yield of hydroxyl radical formation, i.e., the fraction of absorbed photons that result in •OH formation (Eq. (9)). The average (± 1σ) value of Φ_{OH} in all particle extracts is (0.014 ± 0.010) %, which is statistically similar to the average fog result (Table S3): while photoformation rates of •OH increase from fog to standard particle extracts (Table S3), light absorption shows a similar trend (Table S1).

The rate of •OH photoproduction in the field blanks is negligible, representing 1 % and 6 % of the average rate in standard and dilute extracts, respectively. The rate constants for •OH destruction (k'_{OH}) in the standard (FB2) and dilute (FB1) field blanks represent 10 % and 43 % of the corresponding PME averages. The latter result is puzzling, since the concentrations of •OH sinks measured in FB1 (i.e., DOC and NO_2^-; Table S2) are much lower relative to the extract. We discuss measurements of k'_{OH} in the blanks in more detail in Sect. S2. We do not subtract the field blank results for k'_{OH} from the corresponding PM extract values and thus our sample results are upper bounds.

3.4 Singlet molecular oxygen

The average (± 1σ) Davis winter solstice-normalized $^1O_2$* concentration in the dilute extracts (2.4 (± 0.7) × 10^{-13} M) is very similar to the previous fog average (Fig. 2b). This is likely because brown carbon is the source of $^1O_2$* (Faust and Allen, 1992; Zepp et al., 1977) and the DOC concentrations in the fog and dilute extracts are very similar (Table S2). On the other hand, the average [$^1O_2$*] in the more concentrated, standard PM extracts (PME3–6), is 1.6 (± 0.5) × 10^{-12} M, nearly seven times higher than the averages in Davis fog and dilute extracts (Fig. 2b, Table S7). This is because the standard extracts have higher DOC concentrations but the same major $^1O_2$* sink, i.e., water. Across all fog and particle extracts, the rate of singlet oxygen formation (P_{1O2*}) is strongly correlated with the rate of sunlight absorption (R_{abs}) (R^2 = 0.94; Fig. 3a), although this correlation is not evident in only the fog samples (Kaur and Anastasio, 2017).

Similar to •OH, quantum yields of $^1O_2$* are similar in the extracts (standard and dilute) and fog (Table S7); the slope of the P_{1O2*} versus R_{abs} correlation line (Fig. 3a) gives an overall quantum yield of $^1O_2$* of (3.8 ± 0.2) %, i.e., across all samples roughly 4% of the photons absorbed lead to the formation of singlet oxygen. This is nearly 260 times higher than the average quantum yield of •OH.

Atmos. Chem. Phys. Discuss., https://doi.org/10.5194/acp-2018-1258
Manuscript under review for journal Atmos. Chem. Phys.
Discussion started: 10 December 2018

3.5 Triplet excited states of organic matter (^{3}C*)

We also determined the kinetics and concentrations of oxidizing "triplets", by measuring the loss of two probes, syringol (SYR) and methyl jasmonate (MeJA) (Fig. S8). In the standard extracts, the average (± σ) Davis winter-normalized rate constants for loss of SYR and MeJA (k'_{Probe}) are (4.3 ± 1.7) × 10^{-4} s^{-1} and (2.6 ± 0.7) × 10^{-5} s^{-1}, which are equivalent to average lifetimes of 0.70 (± 0.20) and 11 (± 3) h, respectively (Tables S8 and S9). Triplet probe lifetimes in the dilute extracts are approximately three times longer and are very similar to fog values, indicating that the main source of triplet precursors to fog drops is the BrC present in the fog condensation nuclei rather than mass transport from the gas phase.

We correct the loss of triplet probes for oxidation by hydroxyl radical and singlet molecular oxygen (Eq. (6)). In the standard extracts, $^1O_2$* and $^{\bullet}$OH account for an average of 13 % and 3 % of SYR loss, respectively (Table S8, Fig. S9); for methyl jasmonate, the corresponding contributions are 37 % and 12 %.

Next we use the ratio of the pseudo-first-order rate constants for probe losses by triplets, i.e., $k'_{SYR,3C*}$ / $k'_{MeJA,3C*}$, to characterize the average reactivity of the triplet species in each sample: a ratio close to 1 indicates higher reactivity, while a higher ratio indicates lower reactivity. The $k'_{Probe,3C*}$ ratio in all extracts ranges between 15 and 37 (Table S12), which is a narrower range than in Davis fog samples (7.5 to 110) (Kaur and Anastasio, 2018b). Based on the $k'_{Probe,3C*}$ ratios, triplets in the PM extracts generally have an average reactivity similar to model aromatic triplets 3'-methoxyacetophenone (^{3}3MAP*) and 3,4-dimethoxybenzaldehyde (^{3}DMB*) (Fig. 2c, Table S12). The average (± σ) triplet steady-state concentration in the standard extracts is 1.0 (± 0.4) × 10^{-13} M (Fig. 2c, Table S13), which is nearly twice the fog average, but not statistically significantly different. If we consider only the PM and fog samples that have triplet reactivities similar to ^{3}3MAP* and ^{3}DMB* (i.e., the green average lines in Fig. 2c), the average triplet concentration in the standard PM extracts is nearly four times greater than in fog (Table S2), similar to the ratio of DOC concentrations.

In the standard extracts the average concentration of oxidizing triplets is 16 times lower than [$^1O_2$*] but nearly 210 times higher than [$^{\bullet}$OH] from *in situ* sources. Our measurements of oxidizing triplet concentrations lie at the higher end of measured and estimated concentrations of total (i.e., oxidizing and energy transfer) triplets in surface waters, 10^{-15}–10^{-13} M (Zepp et al., 1985; Grebel et al., 2011). The average (± 1 σ) rate of triplet photoformation, P_{3C*}, is 2.0 (± 1.0) × 10^{-7} M s^{-1} (i.e., 720 (± 360) μM h^{-1}) in the standard extracts (Table S13). Thus the ratios of the

467 average production rates for $^1O_2$*, ^{3}C*, and $^{\bullet}$OH are 290 : 170 : 1. There is a fair correlation
468 between P_{3C*} and R_{abs} (Fig. 3b), similar to the case for P_{1O2*} (Fig. 3a), consistent with BrC as the
469 source of triplets. Sample-to-sample variability in the fraction of the total triplet pool that can
470 oxidize organics likely causes the P_{3C*} correlation (R^2 = 0.60) to be weaker than that of P_{1O2*} (R^2
471 = 0.94). The average (± 1σ) oxidizing triplet quantum yield in all extracts is (2.4 ± 1.0) % (Table
472 S13), approximately two times lower than the value for $^1O_2$* (Table S7) but 150 times higher
473 than for $^{\bullet}$OH (Table S3).

474 Triplet excited states have two main reaction pathways: energy transfer (e.g., to make
475 $^1O_2$*) and electron transfer (e.g., to oxidize a phenol) (Zepp et al., 1985; McNeill and Canonica,
476 2016; Kaur and Anastasio, 2018b). Essentially all triplets possess enough energy to form $^1O_2$*
477 (McNeill and Canonica, 2016), but only a subset of the triplet pool can oxidize organics via
478 electron transfer. Thus the quantum yield of $^1O_2$* can be used to estimate the total triplet
479 quantum yield, while our measurements of Φ_{3C*} constrain the smaller subset of oxidizing triplets
480 (assuming energy transfer from triplets is the only source of $^1O_2$*). The quantum yield for all
481 triplets can be estimated as Φ_{1O2*}/f_{Δ}, where f_{Δ}, the fraction of ^{3}C* interactions with dissolved O_2
482 that yield $^1O_2$*, is approximately 0.5 (McNeill and Canonica, 2016; Kaur and Anastasio, 2018b).
483 For our standard extracts, the average value of Φ_{1O2*}/f_{Δ} is 0.078 ± 0.019, i.e., approximately 8 %
484 of the photons absorbed by brown carbon chromophores make a triplet excited state. Next we use
485 the ratio $\Phi_{3C*}/(\Phi_{1O2*}/f_{\Delta})$ to estimate the fraction of all triplets that can participate in electron-
486 transfer (oxidation) reactions. The average value of this fraction is 0.37 ± 0.12 for all the PM
487 extracts, i.e., on average, 37 % of all triplets are oxidizing (range = 18–53 %; Table S13).

488 **3.6 Predicting photooxidant concentrations in ambient particle water**

489 Since our particle extracts are approximately 1000 times more dilute than ambient Davis
490 particles during winter, we want to be able to estimate oxidant concentrations under ambient
491 conditions. To do this we first measured photooxidant concentrations as a function of dilution for
492 the same sample and then extrapolated our results to ambient particle conditions. For the first
493 step, we extracted squares of filter #3 using five different volumes of Milli-Q water, from 10 to
494 0.50 mL (Sect. 2.5.4), corresponding to aqueous PM mass concentration factors (CF) of 0.05
495 (most dilute) to 0.96 (most concentrated) (Eq. (10)). For this sample, these are equivalent to PM
496 mass / water mass ratios typical for dilute to very concentrated cloud or fog drops, i.e., (0.35 –
497 8.4) × 10^{-4} µg-PM / µg-H_2O (Table S14). The rate of light absorption increases linearly with CF

(Fig. 4a), indicating that BrC and other chromophores are efficiently extracted for all Milli-Q volumes employed.

The change in photooxidant concentration with CF depends on how the ratio of sources and sinks varies with dilution. In the case of hydroxyl radical, P_{OH} and k'_{OH} both increase as extracts get more concentrated (i.e., as CF increases), resulting in an $^{\bullet}OH$ concentration that does not change substantially: with a 20-fold increase in the concentration factor, there appears to be a three-fold increase in [$^{\bullet}OH$] (Fig. 4b). While the data suggest a step increase in [$^{\bullet}OH$] between the lowest and highest CF extracts, we believe this is likely noise in the data, and that the hydroxyl radical concentration is essentially independent of PM mass concentration. This idea is consistent with the relatively constant [$^{\bullet}OH$] in our particle extracts relative to fog (Fig. 3a, black dashed lines) and with prior results showing very similar concentrations for rain, cloud, fog, and marine PM extracts (Fig. S7 and Arakaki et al., 2013).

To estimate [$^{\bullet}OH$] in particle liquid water, we use the measured linear dependences of the rate of $^{\bullet}OH$ photoproduction (P_{OH}) and loss rate constant (k'_{OH}) on concentration factor, which corresponds to a measured PM mass / water mass ratio (Fig. S10). Under a typical wintertime, Central Valley ambient particle water condition (1 μg-PM / μg-H_2O), the *in situ* P_{OH} and k'_{OH} are estimated to be 4.1×10^{-6} M s^{-1} and 7.4×10^{9} s^{-1}, respectively (Fig. S10). This extrapolation of only aqueous processes gives an $^{\bullet}OH$ concentration in particle water of 5.5×10^{-16} M (Fig. 5), which is similar to the average of the measurements in Fig. 4b. However, this estimate does not include the contribution of mass transport of gas-phase $^{\bullet}OH$ to the particles. As detailed in Sect. S4, we estimate that the rate of $^{\bullet}OH$ gas-to-particle transport is 1.4×10^{-6} M s^{-1}, i.e., approximately 30 % of the $^{\bullet}OH$ photoformation rate from aqueous sources. Considering both sources of $^{\bullet}OH$ to the particle liquid water gives an $^{\bullet}OH$ steady-state concentration of roughly 1×10^{-15} M.

In the case of singlet oxygen, steady-state concentrations increase proportionally with PM mass concentration factor (Fig. 4c). Our interpretation of this result is that the concentration of $^1O_2$* sources (i.e., BrC) increases proportionally with concentration factor, while the concentration of the main sink for $^1O_2$* (i.e., water) is essentially unchanged. Extrapolating the Fig. 4c result to ambient PM conditions (1 μg-PM / μg-H_2O) gives an $^1O_2$* concentration in particle water of 2.2×10^{-9} M (Table S15, Fig. 5); this is lowered by approximately a factor of 14, to 1.5×10^{-10} M, when evaporation to the gas-phase and quenching by aqueous organic sinks are considered (Sect. S4). While there are no other measurements of $^1O_2$* in particles, similar enhancements in $^1O_2$* concentrations (up to a factor of 10^5) have been found in cases where $^1O_2$*

precursors become highly concentrated, e.g., in liquid-like regions of ice (Bower and Anastasio, 2013) and in regions of hydrophobic CDOM in solution (Latch and McNeill, 2006).

An increase in CF also increases the triplet steady-state concentration (Fig. 4d), but there is greater uncertainty in this trend, in part because there is more uncertainty in measurements of $\Sigma[^3C_i^*]$. The data in Fig. 4d are well fit by a hyperbolic regression where the triplet concentration initially rises more quickly with CF but then approaches a plateau at higher CF values (dashed line). Our interpretation of this behavior is that as CF increases, [DOM] and $P_{^3C^*}$ increase linearly but the dominant triplet sink switches from dissolved O_2 at low CF to DOM at high CF. (Wenk et al., 2011; 2013) have shown that surface water DOM can quench triplets; based on our previous work, we believe that phenols from wood combustion might play this role in our PM extracts (Smith et al., 2014; 2015). As described in Sect. S5, by fitting a kinetic model to our triplet dilution data we estimate that the total (reaction and quenching) rate constant for triplets with DOC in the PME3 extracts is 3.4 (± 0.5) × 10^8 L mol-C^{-1} s^{-1}.

While our interpretation above provides a good fit to the $^3C^*$ data, there is enough uncertainty that it also possible that triplet concentrations increase linearly with CF: as shown by the dotted line in Fig. 4d, a linear fit passes within one standard error of each triplet concentration. This linear fit is also consistent with the linear relationship exhibited by $^1O_2^*$ in Fig. 4c: since the oxidizing triplets account for 18 to 53 % (Table S13) of the total triplet states, if the increase in concentration of oxidizing triplets slows with increasing CF, we would expect to see some curvature in the $^1O_2^*$ data, but this is not apparent in Fig. 4c. Because it is unclear the extent to which the oxidizing triplet concentration increases with particle concentration in the extracts, we consider both of the fits in Fig. 5. These two extrapolations result in oxidizing triplet concentrations under PM conditions (1 µg-PM / µg-H_2O) of 1.7×10^{-13} M (hyperbolic fit) and 1.5×10^{-10} M (linear fit). Taken together with the other oxidant measurements, and considering interactions with the gas phase and organic sinks for $^1O_2^*$ under particle conditions, we estimate a ratio of $^1O_2^*$: $^3C^*$: $^{\bullet}OH$ concentrations in ambient particle water to be approximately 10^5 : 10^5–10^2 : 1.

4 Implications

Our dilution experiments suggest that $^{\bullet}OH$, $^1O_2^*$, and $^3C^*$ behave very differently as the PM/water ratio increases from cloud and fog drop conditions to water-containing particles (Fig. 5). To understand what this implies for the fate of organic compounds, we estimated the gas-

aqueous partitioning and lifetimes of five model organic compounds for both fog and aqueous aerosol (Fig. 6). We consider reactions with two gas-phase oxidants ($^{\bullet}OH$, O_3) and four aqueous-phase oxidants ($^{\bullet}OH$, O_3, $^1O_2$*, ^3C*) (Table S16). Our model organics represent two groups in terms of gas-aqueous partitioning: one group with modest Henry's law constants ($K_H \sim 10^4$ M atm^{-1}) and one with much higher values ($K_H = 10^9 – 10^{11}$ M atm^{-1}) (Fig. 6 and Table S17).

Fig. 6a shows the overall lifetimes of the five model organics and the fraction of each present in fog and PM. For the organics with the lowest K_H values, approximately 10–20 % is present in the aqueous-phase under fog conditions, but almost none is present in the particle liquid water. Consequently, gas-phase reactions dominate their overall lifetimes, which are approximately 2 to 3 hours for both fog and PM conditions. In contrast, the compounds with high K_H values are partitioned strongly to the aqueous phase for both the fog and PM scenarios (Fig. 6a). But due to the overall higher oxidant concentrations in PM, the lifetimes of these organics are predicted to be shorter – sometimes by large factors – in PM than in fog (Fig. 6a, Table S17). Additionally, their main sinks change from fog to PM, shifting from aqueous $^{\bullet}OH$, O_3, and $^1O_2$* in fog to being generally dominated by $^1O_2$* in PM water (Fig. 6b). For example, for tyrosine (compound 3), the predominant sink changes from aqueous O_3 in fog to $^1O_2$* in water-containing particles, while its lifetime decreases from 1.6 h to 0.05 h (Fig. 6b and Table S17).

While triplets are negligible oxidants for individual organics in particles under the conditions of Fig. 6, the picture changes if we move from the Fig. 6 triplet concentration of 1.7×10^{-13} M to the upper-bound concentration obtained by linear extrapolation (1.5×10^{-10} M; Fig. 5). Under this condition aqueous oxidation still dominates the loss of the high-K_H compounds, but ^3C* are the dominant oxidants in PM and organic lifetimes get shorter by factors of 17 to 580 compared to fog (Fig. S11). While there is large uncertainty in the triplet concentrations in PM, Figs. 6 and S11 both indicate that aqueous oxidants can control the fate of highly soluble species in aerosols and that organic lifetimes can be shorter in PM because of an enhancement in oxidant concentrations.

Finally, even if the concentration of oxidizing triplets is at the lower end of our estimate, the formation rate of ^3C* is fast enough – and the fraction of triplets lost via reaction with organics is high enough – that triplets represent, in aggregate, a significant sink for organic compounds in particles. As described in Sect. 3.5, the formation rates for $^1O_2$*, ^3C*, and OH have a ratio of 290 : 170 : 1, respectively, in the PM extracts; based on our dilution experiments (Fig. 4), we expect similar ratios in ambient particle liquid water. Since organic compounds appear to be the major sinks for all three oxidants under ambient particle conditions, and since each oxidant is at steady-

state, the ratio of formation rates is approximately the same as the ratio of total rates of organic compound oxidation by each oxidant. Thus, while the steady-state concentration of $^3C^*$ might be significantly lower than that of $^1O_2^*$ in particle water, both oxidants appear to be similarly important in the overall processing of particulate organics. In contrast, the total rate of oxidation of organics by $^{\bullet}OH$ appears to be 200–300 times slower, although $^{\bullet}OH$ will be relatively more important for less reactive organics. This comparison suggests that understanding the processing of organics in particle water requires including the contributions of both singlet molecular oxygen and triplet excited states.

5 Conclusions and Uncertainties

We have made the first measurements of singlet molecular oxygen and oxidizing triplet states in aqueous extracts of particles, in addition to measuring hydroxyl radical. Under our standard condition, the particle extracts are approximately three times more concentrated than wintertime Davis fog waters. The extracts contain significant amounts of brown carbon, with DOC-normalized mass absorption coefficients between roughly 15,000 and 30,000 cm^2 g-C^{-1} and Absorption Angstrom Exponents of 6.2 to 7.9. Upon absorbing light, BrC and other chromophores in the samples form significant amounts of $^{\bullet}OH$, $^1O_2^*$, and $^3C^*$. While concentrations of $^{\bullet}OH$ in the PM extracts are in the same range as found in fog waters, concentrations of the oxidants derived primarily from BrC – i.e., $^1O_2^*$ and $^3C^*$ – are higher in the extracts compared to in fog by approximately factors of seven and three, respectively.

Dilution experiments indicate that the $^{\bullet}OH$ concentration is essentially independent of the PM mass concentration in solution, consistent with previous results, while $^1O_2^*$ and $^3C^*$ increase with increasing aqueous PM concentration. Extrapolating our findings to the approximately 1000-times more concentrated conditions expected in ambient particle water suggests that hydroxyl radical concentrations in particles will be similar to values in fog and cloud drops but that oxidants formed from illumination of brown carbon will be enhanced in particles, by approximately a factor of 600 for $^1O_2^*$and between a factor of 3 and 3000 for $^3C^*$, relative to fog waters. The higher $^1O_2^*$ concentrations predicted in particles lead to a large decrease in the lifetimes of highly water-soluble organic compounds compared to foggy conditions, even though the liquid water content of the particles is roughly 10^4 times lower than the fog. It is possible that triplets are also more significant oxidants in PM than in fog, but there is too much uncertainty in our data to properly assess their role. In contrast, $^{\bullet}OH$ is important for the oxidation of organics that react only slowly with $^1O_2^*$ and $^3C^*$, but is otherwise a minor oxidant for the organics we

considered since the particulate $^{\bullet}OH$ concentration is quite low and not enhanced relative to fog conditions.

While our results suggest that oxidants derived from brown carbon are very significant in water-containing particles, there are several large uncertainties. Most significantly, because of experimental limitations on the maximum PM concentration in our extracts, we need to extrapolate oxidant measurements over a very large range (approximately a factor of 1000) to predict oxidant levels in ambient water-containing particles. This results in very large uncertainties. As part of this uncertainty, it is difficult to assess how reactions in the particles might suppress concentrations of $^1O_2$* and, especially, ^3C*. It is also difficult to estimate the importance of evaporation as a sink for $^1O_2$* in particles, although we expect this pathway is minor for $^{\bullet}OH$ and ^3C*. Secondly, while calculations suggest that unaccounted oxidants are minor sinks for our triplet probes, if these species are important our triplet concentrations would be biased high. Finally, it is unclear how widely our results, which are for one season and one location, can be applied to other particles containing brown carbon. However, our one sample collected during both daytime (with little biomass burning) and night (with significant biomass burning) had similar reactivity to samples collected only at night. Regardless, since these are the first measurements of $^1O_2$* and $^3C^*$ in particles, strengthening and improving our findings requires more measurements, especially for other seasons and locations. Measurements under much higher aqueous particle mass concentrations, ideally under ambient conditions, are also needed. Despite the uncertainties, our results indicate that BrC-derived photooxidants such as singlet molecular oxygen and organic triplet excited states can be important sinks for organic compounds in atmospheric particles. Currently these oxidants are not included in atmospheric models, although our calculations suggest that $^1O_2$* and $^3C^*$ are important in the processing of highly soluble organic molecules in aerosols.

Competing Interests

The authors declare that they have no conflict of interest.

Author Contribution

CA and RK developed the research goals and designed the experiments. KB lent and set up the sampler, while RK, CA, and WJ collected samples. RK, JL, and SH performed the photochemistry experiments while WJ analyzed ions and OC. RK analyzed the data and prepared the manuscript with contributions from all co-authors. CA reviewed, wrote portions of, and

edited the manuscript. CA and QZ provided supervision and oversight during the experiments and writing.

Data Availability

Light absorption data have been submitted to the data repository Pangaea, cited in the text and are available at https://doi.pangaea.de/10.1594/PANGAEA.896418. Other data are available upon request.

Acknowledgments

We thank Ann Dillner, Alexandra Boris, and April Chaney (UC Davis, Air Quality Research Center) for use of a microbalance, and the National Science Foundation (AGS-1649212), UC Guru Gobind Singh Fellowship, Donald G. Crosby Graduate Fellowship, and James and Rita Seiber International Student Support Award for funding.

Atmos. Chem. Phys. Discuss., https://doi.org/10.5194/acp-2018-1258
Manuscript under review for journal Atmos. Chem. Phys.
Discussion started: 10 December 2018

Atmospheric Chemistry and Physics Discussions

671 **Figures**

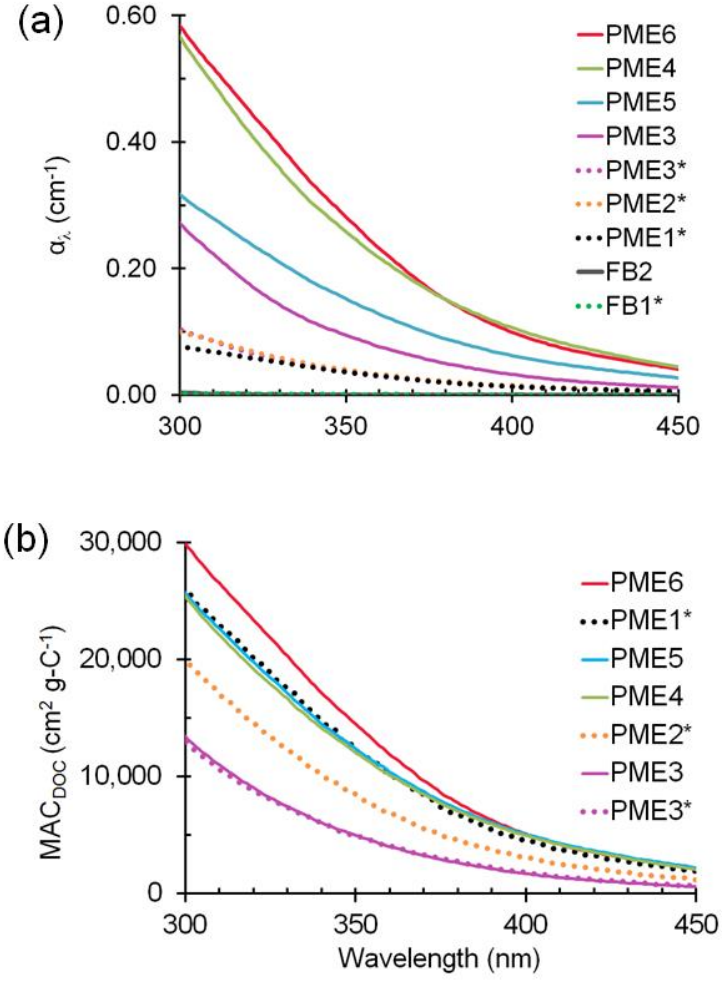

672

673 Figure 1. (a) Light absorption coefficients, α_λ, in particulate matter extracts (PME) (Eq. (1)) and
674 field blanks (FB). The legend shows the sample identities, arranged from the highest absorbing
675 (top) to lowest absorbing (bottom) at 300 nm. Solid and dotted lines represent standard and dilute
676 extracts, respectively (with the latter indicated with an asterisk; Sect. 2.2). (b) Mass absorption
677 coefficients of DOC in the particle extracts (Eq. (3)).

Atmos. Chem. Phys. Discuss., https://doi.org/10.5194/acp-2018-1258
Manuscript under review for journal Atmos. Chem. Phys.
Discussion started: 10 December 2018

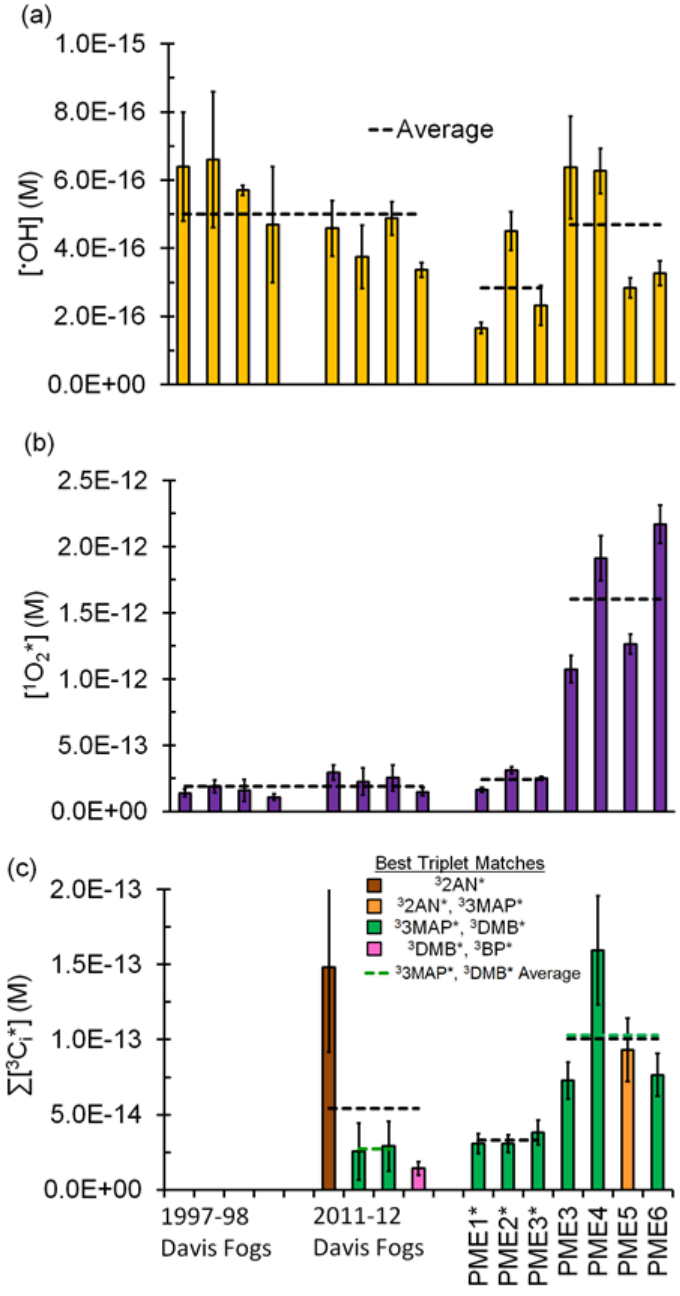

678

679 Figure 2. Measured steady-state concentrations of (a) hydroxyl radical, (b) singlet molecular
680 oxygen and, (c) oxidizing triplet excited states of organic matter in particle extracts, along with
681 previous measurements made in Davis fogs collected between 1997-98 and 2011-12 (Anastasio
682 and McGregor, 2001; Kaur and Anastasio, 2017; Kaur and Anastasio, 2018b). All concentrations
683 are normalized to Davis midday, winter solstice sunlight. Dilute particle extracts are indicated
684 with an asterisk. Dashed lines represent sample averages.

Atmos. Chem. Phys. Discuss., https://doi.org/10.5194/acp-2018-1258
Manuscript under review for journal Atmos. Chem. Phys.
Discussion started: 10 December 2018

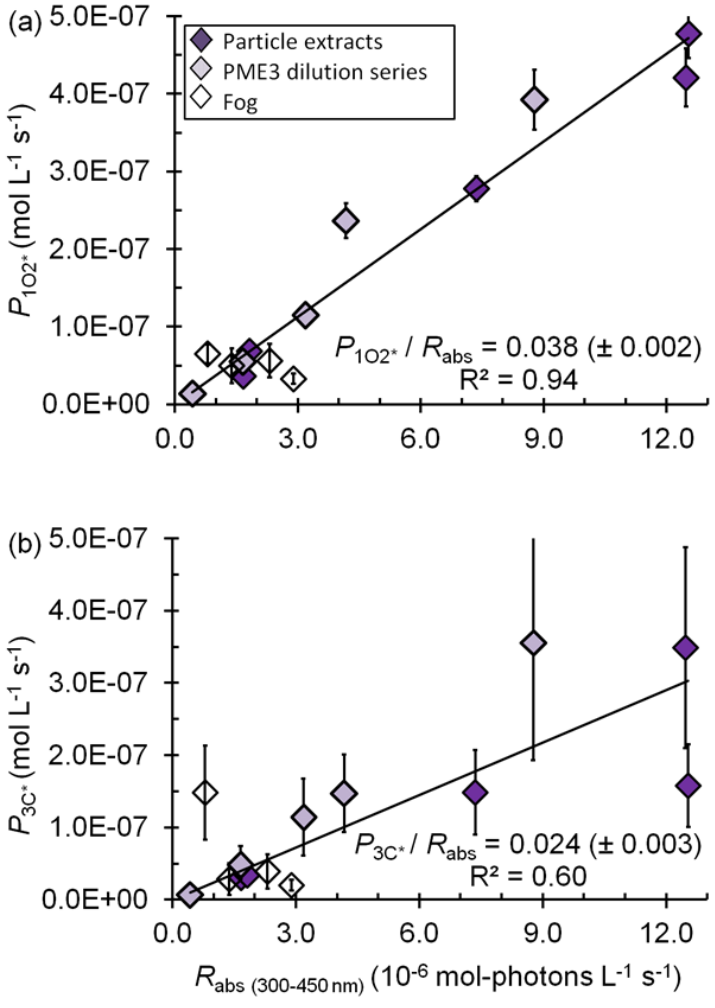

Figure 3. Correlations between (a) the rate of singlet oxygen photoproduction normalized to Davis winter solstice sunlight (P_{1O2^*}), (b) the rate of triplet photoproduction normalized to Davis winter solstice sunlight (P_{3C^*}) and the rate of light absorption (Rabs) between 300 to 450 nm. Triplet rates for the fog samples were adjusted to account for the small DOC sink for triplets; Eq. (8). The P/R_{abs} ratios (± 1 SE) listed are unitless and represent the quantum yields.

Atmos. Chem. Phys. Discuss., https://doi.org/10.5194/acp-2018-1258
Manuscript under review for journal Atmos. Chem. Phys.
Discussion started: 10 December 2018

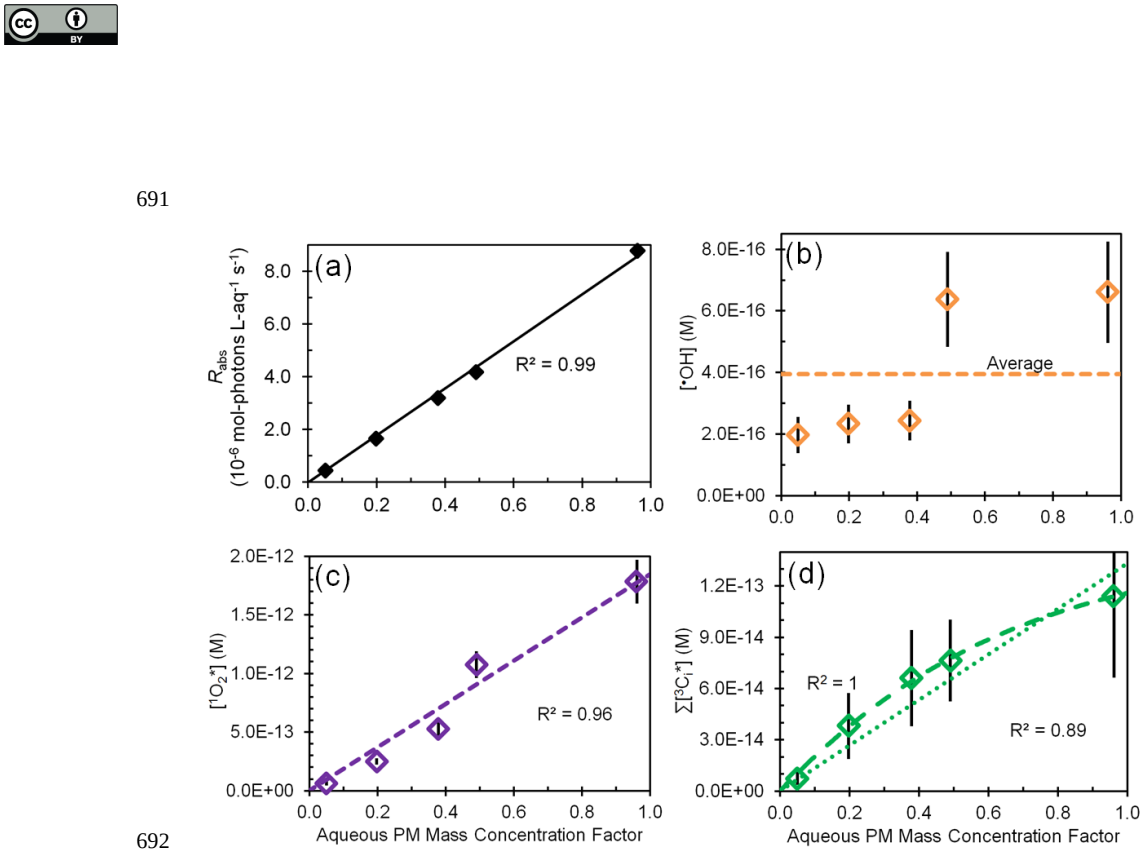

Figure 4. Effect of change in aqueous particle mass concentration (i.e., sample dilution) for sample PME3 on (a) rate of light absorption and the steady-state concentrations of (b) hydroxyl radical, (c) singlet molecular oxygen and, (d) oxidizing triplet excited states of organic matter. The last panel shows both linear (dotted) and hyperbolic (dashed) fits to the data. In each plot the x-axis is a measure of sample dilution, with higher concentration factors corresponding to more concentrated particle extracts (Eq. (10)).

700

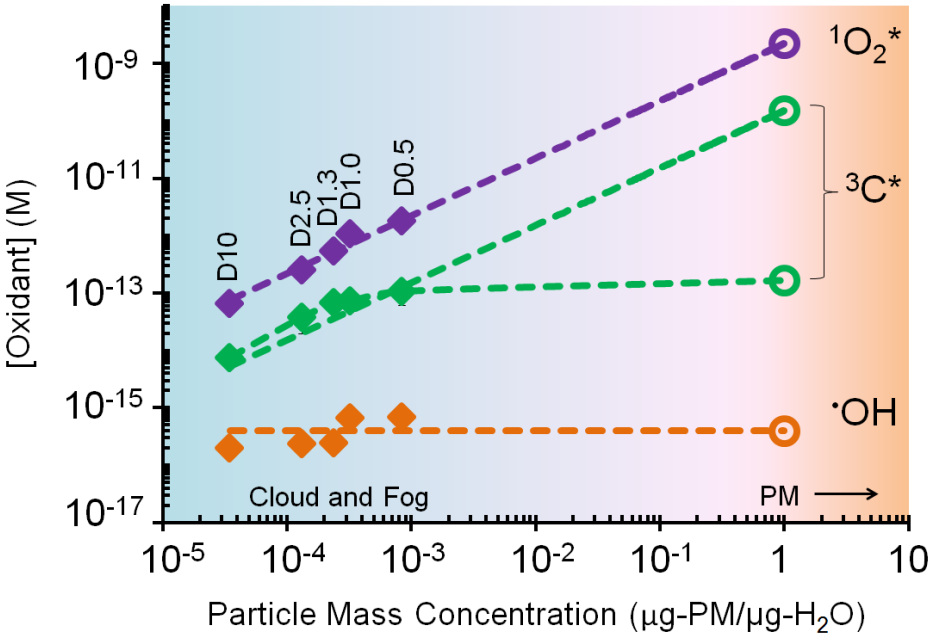

701

702 Figure 5. Dependence of photooxidant concentrations on particle mass concentration in extracts
703 of sample PME3 considering only aqueous-phase processes. Solid diamonds are measured values
704 under experimental dilution conditions (typical for clouds or fogs), while the open circles are
705 values expected in more concentrated particle liquid water based on the dashed line
706 extrapolations. For the solid symbols, error bars (± 1σ) are nearly all smaller than the symbols.
707 Data labels on the diamonds (e.g., D10) represent the water volume used to extract the PME3
708 filter square (Sect. 2.5.4). The impacts of interactions with the gas phase on aqueous
709 concentrations are not included here and are discussed in the text. For oxidizing triplets, two
710 extrapolation scenarios are shown: linear and hyperbolic, representing likely upper and lower
711 bounds of oxidizing triplet concentrations, respectively (Table S15).

Atmos. Chem. Phys. Discuss., https://doi.org/10.5194/acp-2018-1258
Manuscript under review for journal Atmos. Chem. Phys.
Discussion started: 10 December 2018

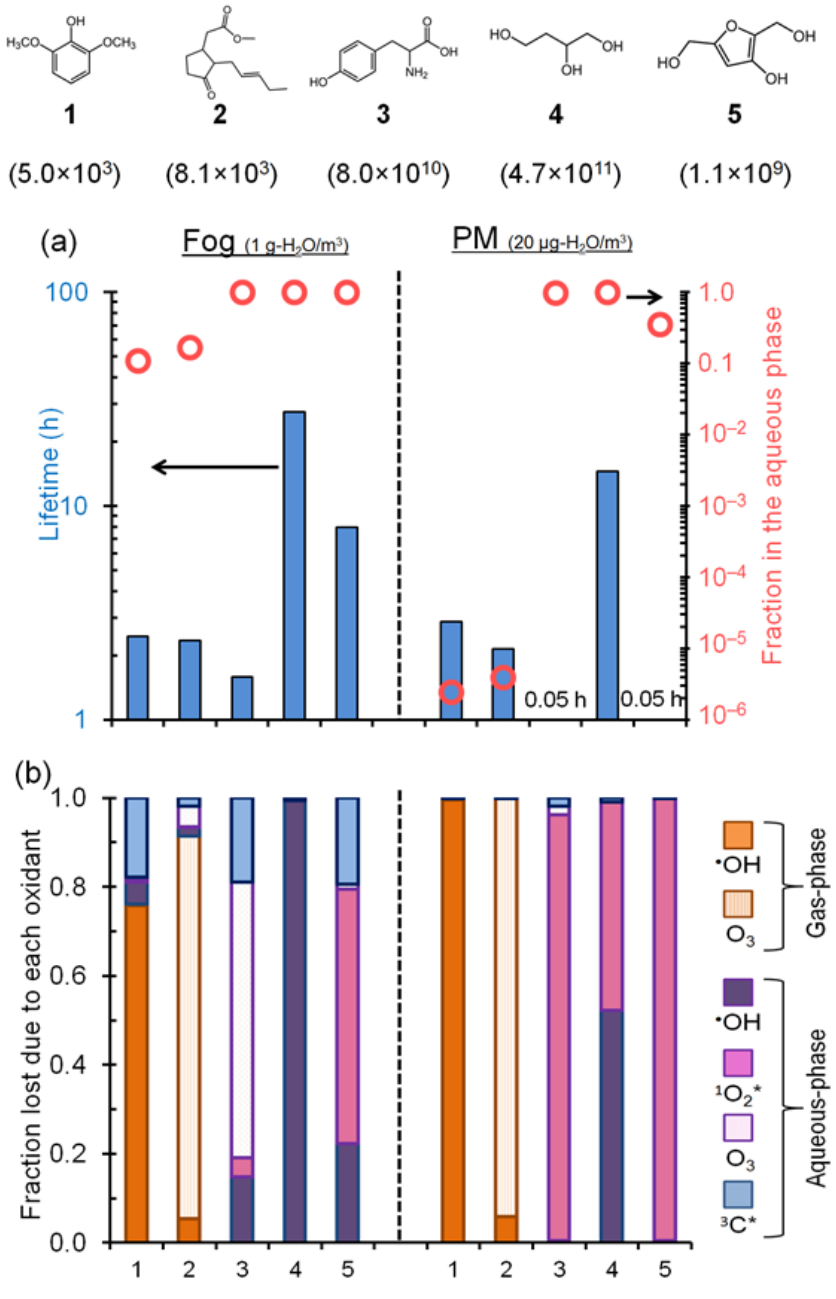

Figure 6. Fate of five model organic compounds – (1) syringol, (2) methyl jasmonate, (3) tyrosine, (4) 1,2,4-butanetriol and (5) 3-hydroxy-2,5-bis(hydroxymethyl)furan – under liquid water content conditions for fog (left of vertical dashed line; 1 g-H_2O / m^3-air) and PM (right of line; 20 µg-H_2O / m^3-air). Estimated Henry's law constants for the compounds (in units of M atm^{-1}) are in parentheses beneath each structure. In panel (a) the columns represent overall lifetimes of the organics and the open circles represent the fractions in the aqueous phase. Panel

719 (b) shows the fraction of each compound lost via various gas and aqueous pathways. The triplet
720 contribution in PM is estimated using the lower-bound triplet concentration extrapolation i.e., 1.7
721 $\times 10^{-13}$ M (Fig. 5). Oxidant concentrations and rate constants are in Tables S16 and S17.

References

Albinet, A., Minero, C., and Vione, D.: Photochemical generation of reactive species upon irradiation of rainwater: Negligible photoactivity of dissolved organic matter, Sci. Total Environ., 408, 3367-3373, 2010.

Anastasio, C., Faust, B. C., and Rao, C. J.: Aromatic carbonyl compounds as aqueous-phase photochemical sources of hydrogen peroxide in acidic sulfate aerosols, fogs, and clouds .1. Non-phenolic methoxybenzaldehydes and methoxyacetophenones with reductants (phenols), Environ. Sci. Technol., 31, 218-232, 1997.

Anastasio, C., and McGregor, K. G.: Chemistry of fog waters in California's central valley: 1. In situ photoformation of hydroxyl radical and singlet molecular oxygen, Atmos. Environ., 35, 1079-1089, 2001.

Anastasio, C., and Jordan, A. L.: Photoformation of hydroxyl radical and hydrogen peroxide in aerosol particles from Alert, Nunavut: Implications for aerosol and snowpack chemistry in the Arctic, Atmos. Environ., 38, 1153-1166, 2004.

Anastasio, C., and Newberg, J. T.: Sources and sinks of hydroxyl radical in sea-salt particles, J. Geophys. Res., 112, D10306, 2007.

Arakaki, T., and Faust, B. C.: Sources, sinks, and mechanisms of hydroxyl radical (˙OH) photoproduction and consumption in authentic acidic continental cloud waters from Whiteface Mountain, New York: The role of the Fe (R)(R= II, III) photochemical cycle, J. Geophys. Res. Atmos., 103, 3487-3504, 1998.

Arakaki, T., Miyake, T., Shibata, M., and Sakugawa, H.: Photochemical formation and scavenging of hydroxyl radical in rain and dew waters, Nippon Kagaku Kaishi, 335-340, 1999.

Arakaki, T., Kuroki, Y., Okada, K., Nakama, Y., Ikota, H., Kinjo, M., Higuchi, T., Uehara, M., and Tanahara, A.: Chemical composition and photochemical formation of hydroxyl radicals in aqueous extracts of aerosol particles collected in Okinawa, Japan, Atmos. Environ., 40, 4764-4774, 2006.

Arakaki, T., Anastasio, C., Kuroki, Y., Nakajima, H., Okada, K., Kotani, Y., Handa, D., Azechi, S., Kimura, T., Tsuhako, A., and Miyagi, Y.: A general scavenging rate constant for reaction of hydroxyl radical with organic carbon in atmospheric waters, Environ. Sci. Technol., 47, 8196-8203, 2013.

Aregahegn, K. Z., Nozière, B., and George, C.: Organic aerosol formation photo-enhanced by the formation of secondary photosensitizers in aerosols, Faraday Discuss., 165, 123-134, 2013.

Bahnmüller, S., von Gunten, U., and Canonica, S.: Sunlight-induced transformation of sulfadiazine and sulfamethoxazole in surface waters and wastewater effluents, Water Res., 57, 183-192, 2014.

Bilski, P., Holt, R. N., and Chignell, C. F.: Properties of singlet molecular oxygen O_2 ($1\Delta g$) in binary solvent mixtures of different polarity and proticity, J. Photochem. Photobiol., A, 109, 243-249, 1997.

Blando, J. D., and Turpin, B. J.: Secondary organic aerosol formation in cloud and fog droplets: A literature evaluation of plausibility, Atmos. Environ., 34, 1623-1632, 2000.

Boreen, A. L., Arnold, W. A., and McNeill, K.: Triplet-sensitized photodegradation of sulfa drugs containing six-membered heterocyclic groups: Identification of an SO_2 extrusion photoproduct, Environ. Sci. Technol., 39, 3630-3638, 2005.

767 Bower, J. P., and Anastasio, C.: Measuring a 10,000-fold enhancement of singlet molecular
768 oxygen (1 O 2*) concentration on illuminated ice relative to the corresponding liquid
769 solution, Atmos. Environ., 75, 188-195, 2013.
770 Brezonik, P. L., and Fulkerson-Brekken, J.: Nitrate-induced photolysis in natural waters:
771 Controls on concentrations of hydroxyl radical photo-intermediates by natural scavenging
772 agents, Environ. Sci. Technol., 32, 3004-3010, 1998.
773 Canonica, S., and Hoigné, J.: Enhanced oxidation of methoxy phenols at micromolar
774 concentration photosensitized by dissolved natural organic material, Chemosphere, 30,
775 2365-2374, 1995.
776 Canonica, S., Jans, U., Stemmler, K., and Hoigne, J.: Transformation kinetics of phenols in
777 water: Photosensitization by dissolved natural organic material and aromatic ketones,
778 Environ. Sci. Technol., 29, 1822-1831, 1995.
779 Canonica, S., Hellrung, B., and Wirz, J.: Oxidation of phenols by triplet aromatic ketones in
780 aqueous solution, J. Phys. Chem. A, 104, 1226-1232, 2000.
781 Canonica, S., Hellrung, B., Müller, P., and Wirz, J.: Aqueous oxidation of phenylurea herbicides
782 by triplet aromatic ketones, Environ. Sci. Technol., 40, 6636-6641, 2006.
783 De Haan, D. O., Corrigan, A. L., Smith, K. W., Stroik, D. R., Turley, J. J., Lee, F. E., Tolbert, M.
784 A., Jimenez, J. L., Cordova, K. E., and Ferrell, G. R.: Secondary organic aerosol-forming
785 reactions of glyoxal with amino acids, Environ. Sci. Technol., 43, 2818-2824, 2009.
786 De Haan, D. O., Hawkins, L. N., Kononenko, J. A., Turley, J. J., Corrigan, A. L., Tolbert, M. A.,
787 and Jimenez, J. L.: Formation of nitrogen-containing oligomers by methylglyoxal and
788 amines in simulated evaporating cloud droplets, Environ. Sci. Technol., 45, 984-991,
789 2010.
790 Dong, M. M., Mezyk, S. P., and Rosario-Ortiz, F. L.: Reactivity of effluent organic matter
791 (EFOM) with hydroxyl radical as a function of molecular weight, Environ. Sci. Technol.,
792 44, 5714-5720, 2010.
793 Ervens, B., Turpin, B., and Weber, R.: Secondary organic aerosol formation in cloud droplets
794 and aqueous particles (aqSOA): a review of laboratory, field and model studies, Atmos.
795 Chem. Phys., 11, 11069-11102, 2011.
796 Faust, B. C., and Allen, J. M.: Aqueous-phase photochemical sources of peroxyl radicals and
797 singlet molecular oxygen in clouds and fog, J. Geophys. Res. Atmos., 97, 12913-12926,
798 1992.
799 Finlayson-Pitts, B. J., and Pitts Jr, J. N.: Chemistry of the upper and lower atmosphere: theory,
800 experiments, and applications, Elsevier, 1999.
801 Galbavy, E. S., Ram, K., and Anastasio, C.: 2-Nitrobenzaldehyde as a chemical actinometer for
802 solution and ice photochemistry, J. Photochem. Photobiol., A, 209, 186-192, 2010.
803 Ge, X., Shaw, S. L., and Zhang, Q.: Toward understanding amines and their degradation
804 products from postcombustion CO_2 capture processes with aerosol mass spectrometry,
805 Environmental Science & Technology, 48, 5066-5075, 2014.
806 Grebel, J. E., Pignatello, J. J., and Mitch, W. A.: Sorbic acid as a quantitative probe for the
807 formation, scavenging and steady-state concentrations of the triplet-excited state of
808 organic compounds, Water Res., 45, 6535-6544, 2011.
809 Haag, W. R., and Gassman, E.: Singlet oxygen in surface waters—part I: Furfuryl alcohol as a
810 trapping agent, Chemosphere, 13, 631-640, 1984.
811 Haag, W. R., and Hoigné, J.: Singlet oxygen in surface waters .3. Photochemical formation and
812 steady-state concentrations in various types of waters, Environ. Sci. Technol., 20, 341-
813 348, 1986.

814 Hawkins, L. N., Welsh, H. G., and Alexander, M. V.: Evidence for pyrazine-based
815 chromophores in cloud water mimics containing methylglyoxal and ammonium sulfate,
816 Atmospheric Chemistry & Physics, 18, 2018.
817 He, C., Liu, J., Carlton, A., Fan, S., Horowitz, L., Levy, I., and Tao, S.: Evaluation of factors
818 controlling global secondary organic aerosol production from cloud processes, Atmos.
819 Chem. Phys., 13, 1913-1926, 2013.
820 Heald, C. L., Collett Jr, J., Lee, T., Benedict, K., Schwandner, F., Li, Y., Clarisse, L., Hurtmans,
821 D., Van Damme, M., and Clerbaux, C.: Atmospheric ammonia and particulate inorganic
822 nitrogen over the United States, Atmos. Chem. Phys., 12, 10295-10312, 2012.
823 Hecobian, A., Zhang, X., Zheng, M., Frank, N., Edgerton, E. S., and Weber, R. J.: Water-Soluble
824 Organic Aerosol material and the light-absorption characteristics of aqueous extracts
825 measured over the Southeastern United States, Atmos. Chem. Phys., 10, 5965-5977,
826 2010.
827 Herner, J. D., Ying, Q., Aw, J., Gao, O., Chang, D. P., and Kleeman, M. J.: Dominant
828 mechanisms that shape the airborne particle size and composition distribution in central
829 California, Aerosol Sci. Technol., 40, 827-844, 2006.
830 Herrmann, H., Hoffmann, D., Schaefer, T., Bräuer, P., and Tilgner, A.: Tropospheric aqueous-
831 phase free-radical chemistry: Radical sources, spectra, reaction kinetics and prediction
832 tools, ChemPhysChem, 11, 3796-3822, 2010.
833 Herrmann, H., Schaefer, T., Tilgner, A., Styler, S. A., Weller, C., Teich, M., and Otto, T.:
834 Tropospheric aqueous-phase chemistry: Kinetics, mechanisms, and its coupling to a
835 changing gas phase, Chem. Rev., 115, 4259-4334, 2015.
836 Hoffer, A., Gelencsér, A., Guyon, P., Kiss, G., Schmid, O., Frank, G., Artaxo, P., and Andreae,
837 M.: Optical properties of humic-like substances (HULIS) in biomass-burning aerosols,
838 Atmos. Chem. Phys., 6, 3563-3570, 2006.
839 Jimenez, J., Canagaratna, M., Donahue, N., Prevot, A., Zhang, Q., Kroll, J. H., DeCarlo, P. F.,
840 Allan, J. D., Coe, H., and Ng, N.: Evolution of organic aerosols in the atmosphere,
841 Science, 326, 1525-1529, 2009.
842 Kaur, R., and Anastasio, C.: Light absorption and the photoformation of hydroxyl radical and
843 singlet oxygen in fog waters, Atmos. Environ., 164, 387-397, 2017.
844 Kaur, R., and Anastasio, C.: Light absorption coefficients of aqueous extracts of wintertime PM
845 collected in Davis, CA, USA., PANGAEA, DOI:
846 https://doi.pangaea.de/10.1594/PANGAEA.896422, 2018a.
847 Kaur, R., and Anastasio, C.: First Measurements of Organic Triplet Excited States in
848 Atmospheric Waters, Environ. Sci. Technol., 52, 5218-5226, 2018b.
849 Kirchstetter, T., and Thatcher, T.: Contribution of organic carbon to wood smoke particulate
850 matter absorption of solar radiation, Atmos. Chem. Phys., 12, 6067-6072, 2012.
851 Laskin, A., Laskin, J., and Nizkorodov, S. A.: Chemistry of atmospheric brown carbon, Chem.
852 Rev., 115, 4335-4382, 2015.
853 Latch, D. E., and McNeill, K.: Microheterogeneity of singlet oxygen distributions in irradiated
854 humic acid solutions, Science, 311, 1743-1747, 2006.
855 Lim, H.-J., Carlton, A. G., and Turpin, B. J.: Isoprene forms secondary organic aerosol through
856 cloud processing: Model simulations, Environ. Sci. Technol., 39, 4441-4446, 2005.
857 Lim, Y., Tan, Y., Perri, M., Seitzinger, S., and Turpin, B.: Aqueous chemistry and its role in
858 secondary organic aerosol (SOA) formation, Atmos. Chem. Phys., 10, 10521-10539,
859 2010.

Lim, Y., and Turpin, B.: Organic peroxide and OH formation in aerosol and cloud water: laboratory evidence for this aqueous chemistry, Atmospheric Chemistry & Physics Discussions, 15, 2015.

Tropospheric ultraviolet-visible model (TUV) version 4.1 http://cprm.acom.ucar.edu/Models/TUV/Interactive_TUV/, 2002

McNeill, K., and Canonica, S.: Triplet state dissolved organic matter in aquatic photochemistry: Reaction mechanisms, substrate scope, and photophysical properties, Environ. Sci. Process. Impact., 18, 1381-1399, 2016.

Parworth, C. L., Young, D. E., Kim, H., Zhang, X., Cappa, C. D., Collier, S., and Zhang, Q.: Wintertime water-soluble aerosol composition and particle water content in Fresno, California, J. Geophys. Res. Atmos., 122, 3155-3170, 2017.

Rossignol, S. p., Aregahegn, K. Z., Tinel, L., Fine, L., Nozière, B., and George, C.: Glyoxal induced atmospheric photosensitized chemistry leading to organic aerosol growth, Environ. Sci. Technol., 48, 3218-3227, 2014.

Seinfeld, J. H., and Pandis, S. N.: Atmospheric chemistry and physics: from air pollution to climate change, John Wiley & Sons, 2012.

Silva, P. J., Liu, D.-Y., Noble, C. A., and Prather, K. A.: Size and chemical characterization of individual particles resulting from biomass burning of local Southern California species, Environ. Sci. Technol., 33, 3068-3076, 1999.

Smith, J. D., Sio, V., Yu, L., Zhang, Q., and Anastasio, C.: Secondary organic aerosol production from aqueous reactions of atmospheric phenols with an organic triplet excited state, Environ. Sci. Technol., 48, 1049-1057, 2014.

Smith, J. D., Kinney, H., and Anastasio, C.: Aqueous benzene-diols react with an organic triplet excited state and hydroxyl radical to form secondary organic aerosol, Phys. Chem. Chem. Phys., 17, 10227-10237, 2015.

Sun, H. L., Biedermann, L., and Bond, T. C.: Color of brown carbon: A model for ultraviolet and visible light absorption by organic carbon aerosol, Geophys. Res. Lett., 34, L17813, 2007.

Thompson, A. M.: The oxidizing capacity of the Earth's atmosphere: Probable past and future changes, Science, 256, 1157-1165, 1992.

Tong, H., Arangio, A. M., Lakey, P. S., Berkemeier, T., Liu, F., Kampf, C. J., Brune, W. H., Pöschl, U., and Shiraiwa, M.: Hydroxyl radicals from secondary organic aerosol decomposition in water, Atmos. Chem. Phys., 16, 1761-1771, 2016.

Tong, H., Lakey, P. S., Arangio, A. M., Socorro, J., Kampf, C. J., Berkemeier, T., Brune, W. H., Pöschl, U., and Shiraiwa, M.: Reactive oxygen species formed in aqueous mixtures of secondary organic aerosols and mineral dust influencing cloud chemistry and public health in the Anthropocene, Faraday Discuss., 200, 251-270, 2017.

Tratnyek, P. G., and Hoigné, J.: Photo-oxidation of 2,4,6-trimethylphenol in aqueous laboratory solutions and natural waters: Kinetics of reaction with singlet oxygen, J. Photochem. Photobiol., A, 84, 153-160, 1994.

Tsui, W. G., Rao, Y., Dai, H.-L., and McNeill, V. F.: Modeling photosensitized secondary organic aerosol formation in laboratory and ambient aerosols, Environ. Sci. Technol., 51, 7496-7501, 2017.

USGS: U.S. Geological Survey. Water Properties - Dissolved Oxygen. Available at https://water.usgs.gov/edu/dissolvedoxygen.html [last accessed: January 23, 2018], 2018.

Varga, B., Kiss, G., Ganszky, I., Gelencsér, A., and Krivacsy, Z.: Isolation of water-soluble organic matter from atmospheric aerosol, Talanta, 55, 561-572, 2001.

907 Wenk, J., Von Gunten, U., and Canonica, S.: Effect of dissolved organic matter on the
908 transformation of contaminants induced by excited triplet states and the hydroxyl radical,
909 Environ. Sci. Technol., 45, 1334-1340, 2011.
910 Wenk, J., Eustis, S. N., McNeill, K., and Canonica, S.: Quenching of excited triplet states by
911 dissolved natural organic matter, Environ. Sci. Technol., 47, 12802-12810, 2013.
912 Wilkinson, F., Helman, W. P., and Ross, A. B.: Rate constants for the decay and reactions of the
913 lowest electronically excited singlet-state of molecular-oxygen in solution - an expanded
914 and revised compilation, J. Phys. Chem. Ref. Data, 24, 663-1021, 1995.
915 Young, D. E., Kim, H., Parworth, C., Zhou, S., Zhang, X., Cappa, C. D., Seco, R., Kim, S., and
916 Zhang, Q.: Influences of emission sources and meteorology on aerosol chemistry in a
917 polluted urban environment: results from DISCOVER-AQ California, Atmos. Chem.
918 Phys., 16, 5427-5451, 2016.
919 Yu, L., Smith, J., Laskin, A., Anastasio, C., Laskin, J., and Zhang, Q.: Chemical characterization
920 of SOA formed from aqueous-phase reactions of phenols with the triplet excited state of
921 carbonyl and hydroxyl radical, Atmos. Chem. Phys., 14, 13801-13816, 2014.
922 Yu, L., Smith, J., Laskin, A., George, K. M., Anastasio, C., Laskin, J., Dillner, A. M., and
923 Zhang, Q.: Molecular transformations of phenolic SOA during photochemical aging in
924 the aqueous phase: competition among oligomerization, functionalization, and
925 fragmentation, Atmos. Chem. Phys., 16, 4511-4527, 2016.
926 Zepp, R. G., Wolfe, N. L., Baughman, G. L., and Hollis, R. C.: Singlet oxygen in natural waters,
927 Nature, 267, 421-423, 1977.
928 Zepp, R. G., Schlotzhauer, P. F., and Sink, R. M.: Photosensitized transformations involving
929 electronic energy transfer in natural waters: role of humic substances, Environ. Sci.
930 Technol., 19, 74-81, 1985.
931 Zhou, X., and Mopper, K.: Determination of photochemically produced hydroxyl radicals in
932 seawater and freshwater, Mar. Chem., 30, 71-88, 1990.

933